Catal Lett (2007) 119:126–133
DOI 10.1007/s10562-007-9209-3

Nanocrystalline CeO_2 in SBA-15: Performance of Pt/CeO_2/SBA-15 Catalyst for Water-gas-shift Reaction

Ya Dong Bi · Wei Zhang · Heng Yong Xu · Wen Zhao Li

Received: 14 April 2007 / Accepted: 9 July 2007 / Published online: 25 July 2007

Abstract CeO_2 particles confined within the pores of an SBA-15 mesoporous silica host were prepared by incipient wetness impregnation (IMP) and deposition precipitation (DP) methods. The materials were characterized by XRD, N_2-adsorption and temperature programmed reduction (TPR) to evaluate the structure, texture, and redox properties. The preparation procedure had significant impact on the assembling mode of CeO_2 inside the SBA-15 mesopores. A high dispersion of CeO_2 particles was achieved via DP, whereas the dispersion of CeO_2 prepared by IMP was found to be inhomogeneous and CeO_2 partially blocked the pores. The CO conversion in the water-gas-shift reaction was enhanced over 1 wt% Pt supported on CeO_2-modified SBA-15 obtained by DP.

Keywords Nanocrystalline CeO_2 · SBA-15 · Pt · Water-gas-shift reaction

1 Introduction

The heterogeneously catalyzed water-gas-shift reaction (WGSR) ($CO + H_2O \Leftrightarrow CO_2 + H_2$) is a key step in fuel processing to generate H_2. At present, there is a renewed interest in the WGS reaction for the complete conversion of CO to manufacture highly purified hydrogen for PEM fuel cells [1]. The new generation of WGSR catalysts should combine both high activity and structural stability in air and during cyclic operation [2]. The commercially available low-temperature WGS catalysts do not meet these stringent requirements yet. Ceria supported noble metal (NM) catalysts have been investigated extensively in recent years as promising next generation WGSR catalysts [3–5].

A key to the development of an advanced catalyst lies in understanding the nature of the active sites. While the nature of active sites for WGS on supported NM catalysts is still being elucidated, increasing experimental evidence shows that the interaction between NM particles and the oxide support at their contact interface plays an important role in determining the catalytic activity [6, 7]. Xu et al. [8] reported the effect of nanosized ZrO_2 on the activity of Au/ZrO_2 catalysts, which exhibit excellent catalytic performance for CO oxidation showing that the catalytic activity of Au nanoparticles in Au/ZrO_2 can be greatly improved by reducing the particle size of the zirconia nanoparticles. Corma's group [9] reported that the properties of a CeO_2 support can change drastically when the particle size is decreased to the nanosize region. Panagiotopoulou et al. [10] investigated the effect of the morphology of the TiO_2 support on WGS reaction performance of Pt/TiO_2 catalysts and found that the turnover frequency of CO increased exponentially with decreasing the primary crystallite size of TiO_2 due to a substantial decrease of the apparent activation energy. It is known that a synergetic effect between the CeO_2 support and Pt may exist at the interface such that the CeO_2 does not simply act as an inert carrier, but intervenes in the catalytic process. It can be expected that such interaction can be tuned by systematically reducing the particle size of the support oxides.

The recent breakthrough in the synthesis of mesoporous materials has led to a new class of materials with a high

Y. D. Bi · H. Y. Xu (✉) · W. Z. Li
Applied Catalysis Laboratory, Dalian Institute of Chemical Physics, Chinese Academy of Sciences, Dalian 116023, China
e-mail: xuhy@dicp.ac.cn

W. Zhang
Department of Chemistry, Harbin Normal University, Harbin 150080, China

degree of control of the pore size and shape [11]. Ordered mesoporous silica (OMS) is considered as an ideal host for nanoparticles due to its large surface area and well-defined pore structure [12]. Various guest phases such as metals [13], metal oxides [14], sulfides [15] and others have been successfully assembled in the pore systems of OMS.

All the above potential positive effects of CeO_2 on the preparation of Pt-supported catalysts should be enhanced if one were able to prepare high surface area and well structured CeO_2 supports. To create high surface area materials, investigations were initiated on supporting CeO_2 on ordered mesopores oxides, because the pores of OMS could prevent the particles from growing larger than the pores size. The very high surfaces of OMS offer new possibilities for obtaining highly dispersed metal oxide species. In the present work, we employed SBA-15 as a host to confine CeO_2 nanoparticles using different procedures. SBA-15 is a stable OMS for forming embedded nanoparticles due to its thick wall and excellent hydrothermal stability; furthermore its uniform pore size (in the range of 5–30 nm) is interesting for catalysis [16].

2 Experimental

2.1 Catalyst Preparation

SBA-15 was purchased from Jilin University HighTech. CeO_2 was inserted into SBA-15 by two methods: incipient wetness impregnation (IMP) and deposition precipitation (DP). The CeO_2-modified SBA-15 supports are denoted by their preparation method (IMP and DP), with the digits specifying the CeO_2 content (wt%).

The insertion of CeO_2 into SBA-15 by IMP method was carried out by IMP of the support with an aqueous solution of cerium (IV) ammonium nitrate with an appropriate concentration. The solvent was evaporated at 343 K followed by drying of the sample at 393 K and calcination in a muffle furnace at 773 K for 4 h.

The insertion of CeO_2 into SBA-15 by DP was carried out by homogeneous precipitation of cerium hydroxide inside the silica mesopores. In a typical preparation, 1.6 g of SBA-15 was put into a round bottom flask thermostated at 363 K. Urea (0.372 M) was added to 100 mL of an aqueous solution of cerium (IV) ammonium nitrate (0.023 M). The suspension was magnetically stirred while refluxing it using a condensator. After 150 min of deposition–precipitation the suspension was cooled to RT and then filtered. Then the sample was washed with hot deionized water for three times. Finally the sample was dried at 120 °C for 24 h and calcined at 773 K for 4 h. Unsupported CeO_2 was also prepared by the same procedure, with the DP step performed in the absence of SBA-15.

Pt was deposited on the ceria-modified SBA-15, as well as pure SBA-15 and unsupported CeO_2 reference support. In a typical preparation, 1 g of support was immersed into 10 mL of an aqueous solution of H_2PtCl_6 to obtain a final Pt content of 1 wt%. The solvent was evaporated at 343 K followed by drying at 393 K and calcination in a muffle furnace at 773 K for 4 h.

2.2 Catalyst Characterization

X-ray powder diffraction (XRD) patterns of the prepared samples were measured on a Philips CM-1 (Cu Kα, $\lambda = 0.1543$ nm) powder X-ray diffractometer. Typically, the data was collected from 10° to 80° (2θ) for conventional wide-angle XRD patterns. The software X'Pert High score was used to perform microstructure analysis. The particle sizes of the powdered samples were calculated from the diffraction patterns using the Scherrer formula.

BET surface area, Pore size distribution (PSD) and pore volume were measured by the physisorption method using nitrogen as absorbent (Quantachrome NOVA4000). The specific surface area S_{BET} was determined from the linear portion of the BET plot. The PSD was calculated from the adsorption and desorption branch of the N_2 adsorption isotherm using the Barrett–Joyner–Halenda (BJH) formula. The total pore volume was calculated by means of the total amount of adsorbed gas at $P/P_0 = 0.98$. Prior to the surface area and PSD measurements, the samples were degassed in vacuum at 573 K for 3 h to remove physically adsorbed components.

Temperature-programmed reductions (TPR) were carried out in a conventional setup equipped with a programmable temperature furnace. About 40 mg of each sample was introduced into a tubular quartz reactor. Each sample was first treated at 723 K for 30 min and then cooled down to room temperature in Ar. TPR experiments were performed under a flow of 5% H_2/Ar (30 mL/min) from 293 to 1,173 K at a constant heating rate (10 K/min). The consumption of hydrogen was monitored with a thermal conductivity detector (TCD). The H_2 uptake was calibrated by the reduction of CuO.

2.3 Reaction Activity

The catalytic activity measurements were performed in a fixed-bed continuous flow quartz reactor (8 mm i.d.) at atmospheric pressure. The flows of inlet gases (CO, He) were controlled by mass-flow controllers (MFC). A syringe pump (Elite Crop.) was used for feeding water. Water was pumped into a vaporizer where it was vaporized and heated to 498 K and mixed with the gas stream coming from the MFC. The reaction temperature was controlled by a programmable temperature controller and detected by a

movable thermocouple inside the catalyst bed. A gas chromatograph (Shimadzu, GC-8A), equipped with a carbon molecular sieve column and a TCD was used to analyze the products.

To determine the relative reactivity of each catalyst, a 100 mg sample was used in each run and the total flow rate of feed gases was 200 mL/min. All samples were used in the as prepared form without activation. In a typical experiment, the catalyst was heated to 623 K under He flow and then the flow was switched to the reaction mixture, which consisted 4% CO + 12% H_2O in He. The catalyst was conditioned at this temperature for 1 h and then the conversions of reactants were analyzed. Similar measurements were performed following the stepwise lowering of temperature.

3 Results and Discussion

3.1 Structural XRD Characterization

Figure 1 shows the wide-angle XRD patterns of CeO_2-modified and pristine SBA-15 samples. The pure SBA-15 sample showed only one broad diffraction peak of amorphous silica centered at about $2\theta = 23°$. The wide-angle XRD patterns of CeO_2/SBA-15 prepared by both IMP and DP methods showed full set of peaks corresponding to a cubic ceria phase besides amorphous silica. The average nanocrystal size, calculated from the <220> peak using the Scherrer equation, was 7.3 nm for IMP while 2.9 nm for DP, respectively, when both samples contained 20 wt% CeO_2. Ceria dispersion by IMP gave larger crystallites than that by the DP method. In the view of preparation process, the main difference between IMP and DP is that in IMP the formation of CeO_2 occurs in the bulk of the solvent filled within the SBA-15 pores, while in DP includes an intermediate step i.e. precipitation of cerium hydroxide that probably strongly interacts with SBA-15 pore walls surface [17]. Thus, during IMP the interaction of the Ce-phase with the silica surface is much weaker than that during DP. The IMP method therefore is not appropriate for preparing highly dispersed CeO_2 species.

The DP process must be applied with care due to the interaction between metal precursors and the silica surface. For example, when metals such as Ni or Co are precipitated on SBA-15, this type of interaction could lead to the formation of metal silicates and the contraction of the pore wall. Nevertheless, the pores of SBA-15 have rather thick walls, so the DP method still could be applied without severe destruction of the pore structure. It was possible to preserve the pore structure of SBA-15 after supporting a high loading of Ni through the DP method [18]. Recently, SBA-15 has been functionalized with Co by the DP procedure [19]. The presence of cerium silicate has been reported in case of cerium-containing mordenites prepared by in situ incorporation. However, the characteristic peaks of cerium silicate were not observed for our sample, which showed that no crystalline silicate phases were formed.

3.2 Texture of CeO_2/SBA-15 Supports

Figure 2 shows the N_2 adsorption/desorption isotherms for CeO_2-modified and pristine SBA-15 samples. Three different regions can be seen on these isotherm plots [20]: (i) a linear region due to monolayer–multilayer adsorption in mesopores; (ii) a steep region due to capillary condensation within these mesopores; (iii) a second linear region due to multilayer formation on the external surface of the grains.

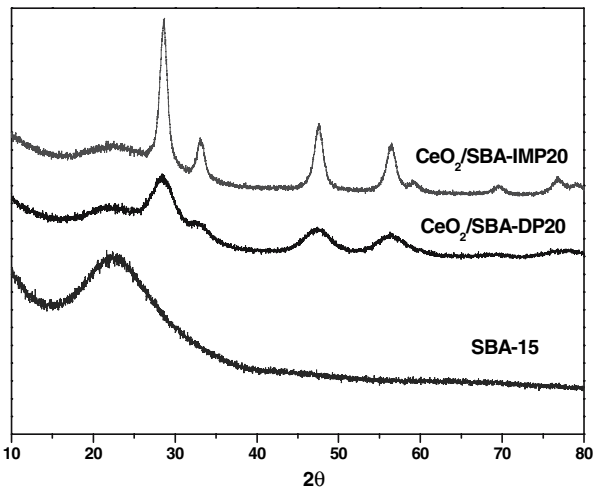

Fig. 1 Wide-angle XRD patterns of CeO_2-modified and pristine SBA-15

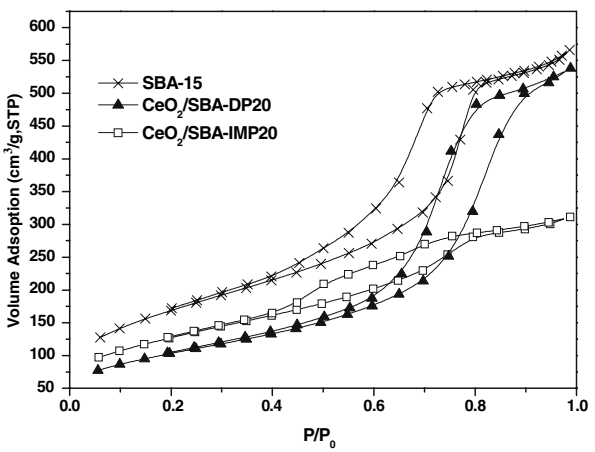

Fig. 2 N2 adsorption-desorption isotherms of CeO2-modified and pristine SBA-15

The isotherm of the SBA-15 sample is of type IV with a H1 type hysteresis loop. Loading of CeO_2 into SBA-15 led to a marked change in the pore structure. For the IMP sample, a hysteresis loop was observed at relative pressures P/P_0 between 0.4 and 0.85, where the increase is not as sharp as for the parent SBA-15 and the DP sample. The hysteresis loop of the IMP sample is characteristic of a percolation effect [21] caused by small CeO_2 nanocrystals settling within the mesopores and effectively forming ink-bottle type pores, indicating the presence of pores that are very narrow at the entrances. For the DP sample, the shape of the hysteresis loop closely resembled that of the pristine SBA-15; therefore the framework did not break down during the DP process. Nevertheless, the relative pressure (P/P_0) at which the hysteresis loop begins to increase indicates an increase of mesopore diameters. As observed by the XRD results above, there is no cerium silicate present in the DP sample, so the DP procedure itself is therefore affecting the initially ordered hexagonal structure of SBA-15.

Figure 3 shows the PSD calculated from the adsorption branch of the isotherms using the BJH method. The position of the distribution maximum is affected by the DP procedure, i.e. the pore size of the samples is increasing with the incorporation of CeO_2. The increase in pore size indicates that the pore wall thickness is decreasing, because the silica walls are contracting during the DP process. The PSD for the IMP sample is shifted to lower pore diameters with CeO_2 loading, reflecting the filling of SBA-15 pores by CeO_2 nanocrystals.

Table 1 lists the surface area, pore volume, pore diameter and micropore volume. The BET surface area decreases significantly with CeO_2 incorporation. There is a significant difference in the pore volume and BJH pore diameter of CeO_2/SBA-15 prepared by different methods. For the CeO_2/SBA-IMP20 sample, the adsorbed volume and BJH pore diameter are strongly reduced, and therefore part of the pore system is presumably blocked. For the CeO_2/SBA-DP20 sample, the pore volume is practically retained with a relatively high value of 0.8271 cm^3/g. If the increase in specific density due to the incorporation of the heavy element cerium is taken into account, the total pore volume is in fact increasing, which also verifies the contraction of the pore walls.

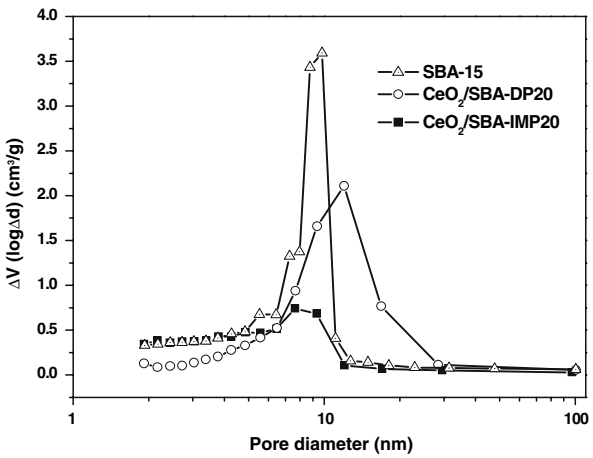

Fig. 3 Pore size distribution (PSD) of CeO2-modified and pristine SBA-15 calculated from the adsorption branch of the isotherms using the BJH method

It is well known in the literature that SBA-15 contains some micropores, which are interconnecting the hexagonal mesopores. From the micropore volume data listed in Table 1, it can be seen that the decrease in microporosity for the CeO_2/SBA-DP20 sample is remarkable. But for the CeO_2/SBA-IMP20 one, there is no obvious change in microporosity. Figure 4 compares *t*-plot curves of samples SBA-15, CeO_2/SBA-DP20, and CeO_2/SBA-IMP20. If the *t*-plot curve is a straight line passing through the origin, there is no microporosity in the samples, while a deviation from such a straight line indicates microporosity [22]. The microporosity of the CeO_2/SBA-DP20 sample is greatly reduced, as its *t*-plot curve is almost a straight line passing near the origin, while the *t*-plot curves of both SBA-15 and CeO_2/SBA-IMP20 greatly deviate from the origin. We believe that these micropores are not actually disappearing; instead they are being transformed into mesopores due to the contraction of the pore walls. A similar result was reported in one study of post-synthesis basic treatment of SBA-15, where both micropores and mesopores are enlarged and marcropores connecting ordered mesopores are detected after an ammonia treatment at 373 K [23].

3.3 Temperature Programmed Reduction of CeO_2/SBA-15 Supports

The redox behavior of the CeO_2/SBA-15 supports in the presence and absence of Pt were studied by TPR. Figure 5 shows the TPR profiles (hydrogen consumption against temperature) of the mesoporous SBA-15 supported CeO_2 and Fig. 6 shows those of the corresponding Pt/CeO_2/SBA-15 catalysts (1 wt% Pt).

The preparation methods have a significant impact on the TPR profiles. The CeO_2/SBA-DP20 support exhibits two reduction peaks, the first one at low (812 K) temperature and the second one at high (980 K) temperature. This behavior is in agreement with previously reported CeO_2 reduction [24], with a low temperature reduction peak (at ca. 770 K) attributed to the reduction of the most easily reducible surface-capping oxygen of ceria and the second high-temperature peak (at ca. 1,100 K) attributed to the bulk reduction of CeO_2. It is worth mentioning the relatively high amount of hydrogen consumed in the low-

Table 1 The physical properties of CeO_2-modified and pristine SBA-15

Sample	S_{BET} (m^2/g)[a]	Pore volume (mL/g)[b]	Pore diameter (nm)[c]	Micropore volume (cm^3/g)[d]
SBA-15	610	0.8697	8.783	0.020
CeO_2/SBA-IMP20	458	0.4787	1.915	0.012
CeO_2/SBA-DP20	373	0.8271	9.364	0.003

[a] Calculated from the linear portion of the BET plot

[b] Calculated from the total amount of adsorbed gas at $P/P_0 = 0.98$

[c] Calculated from the BJH adsorption pore diameter

[d] Calculated by the *t*-plot method

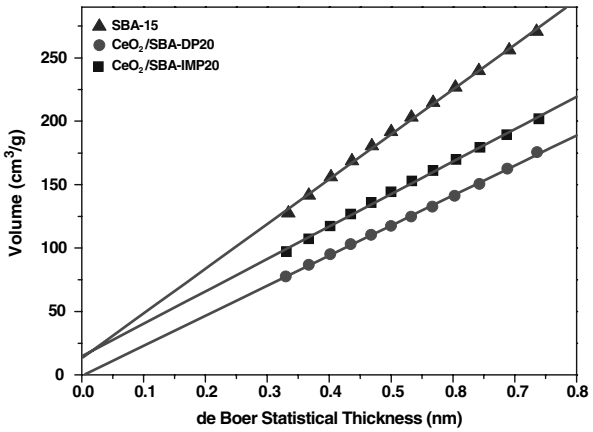

Fig. 4 *t*-Plot profiles of CeO2-modified and pristine SBA-15

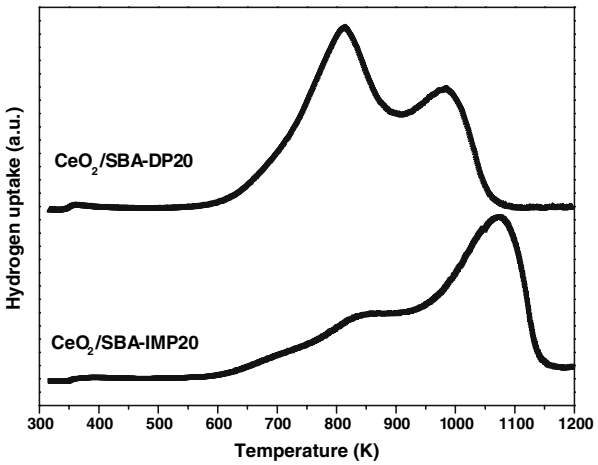

Fig. 5 Temperature-programmed reduction (TPR) profiles of CeO2-modified SBA-15

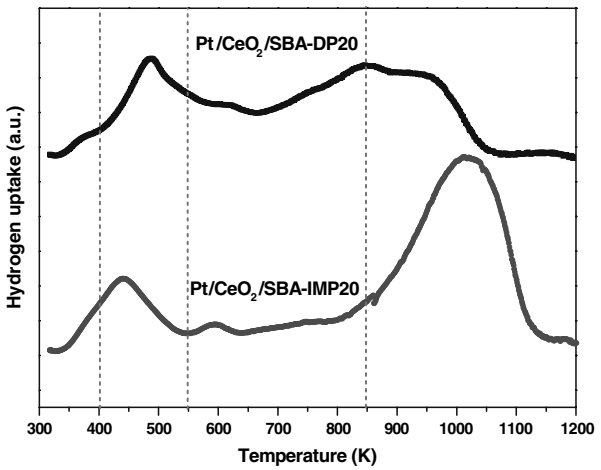

Fig. 6 Temperature-programmed reduction (TPR) profiles of Pt catalyst supported on CeO2-modified SBA-15

temperature reduction peak with respect to the bulk process. This phenomenon can be related to the high proportion of surface CeO_2 species in the nanoparticles present in the support. The bulk reduction temperature (980 K) is downward shifted by 120 K compared with that reported in the literature. Trovarelli [25] suggested the crystallite sizes are the critical factors in determining the TPR properties of ceria particles. With this in mind, the improvement in reducibility would be associated with the high dispersion of CeO_2 when supported on SBA-15 during the DP process.

For the CeO_2/SBA-IMP20 support, there is a small shoulder peak at low temperature (712 K) and a main peak centered at 879 K, which are assigned to surface ceria reduction and suggest a larger variation of the ceria particle size distribution. This further confirmed that the dispersion of CeO_2 by IMP method was heterogeneous. As for the bulk reduction peak, the reduction temperature is increased to 1,071 K, which is similar to that of conventional bulk ceria. In contrast to CeO_2/SBA-DP20, the most of hydrogen was consumed at high temperature and not in the surface reduction process.

The incorporation of Pt into the CeO_2/SBA-15 support completely changes the TPR profiles. The shape of both TPR profiles is composed of many overlapping peaks, which are difficult to decovolute. According to the main peak positions in the TPR spectra, we tentatively consider four types of reducible species. Firstly, the shoulder peak for hydrogen consumption at low temperature (below 400 K) is attributed to the reduction of oxidized Pt to Pt^0. This reduction process must be associated with noble metal

particles that are not subjected to a strong metal-support interaction, i.e. Pt particles that are present on the silica. The small hydrogen consumption associated with this reduction peak would be also an indication for the preferential adherence of Pt particles to CeO_2 nanoparticles. Corma [26] also demonstrated the preference of Pt anchoring on CeO_2 instead of SiO_2 in a CeO_2–SiO_2 material due to the presence of metal–ceria interactions. The surface properties of supports play a key role in the successful incorporation and dispersion of nanoparticles on porous oxide supports during the impregnation process [27]. The prerequisite for the deposition of Pt (IV) precursors is the interaction of the anionic platinum precursor complexes with a positively charged or neutral oxide surface. However, the rather low isoelectric point (IEP) of silica (~2) implies that surfaces are highly negatively charged under IMP conditions. Compared to silica, the higher IEP component ceria (~6.75) can adsorb the anionic Pt precursor more easily, leading to stronger interaction. Secondly, the hydrogen consumption in the range of 400–550 K was assigned to surface reduction of CeO_2 in close contact with noble metal particles. The reduction of the surface oxygen on ceria is facilitated by Pt due to hydrogen spillover from the exposed metal surface [28]. For the Pt/CeO_2/SBA-DP20 catalyst, this type of Pt–O–CeO_2 associated reduction peak is centered at 485 K, slightly higher than that of the Pt/CeO_2/SBA-IMP20 catalyst (441 K), suggesting a stronger interaction between Pt and CeO_2 particles with reduced crystallite size. Thirdly, the weak reduction process occurring in the broad range from 550 to 850 K can be related to the surface reduction process of ceria not in close contact with Pt. Because part of the surface CeO_2 was reduced at lower temperature, the hydrogen consumption is greatly reduced in this range. Finally, the high temperature reduction peaks are associated with the bulk reduction of ceria, which is almost unaffected by the noble metals presence.

3.4 WGS Reaction Activity Evaluation

The catalytic data of the WGS reaction at GHSV 120,000 mL/(g*h of catalyst) for the reactants CO:H_2O:He = 4:12:84 are given in Fig. 7, plotting the CO conversion over the different catalysts against the reaction temperature. In order to quantify the effects of CeO_2 and SBA-15, the reference catalyst Pt/SBA-15 and Pt/CeO_2 were also tested for comparison. The activity of Pt/SBA-15 catalyst was rather low in whole temperature range of 500–630 K. The catalyst Pt/CeO_2/SBA-IMP20 displayed almost the same activity as the catalyst Pt/CeO_2, which suggested no improvement of ceria dispersion when depositing ceria to SBA-15 by the method of IMP compared to bulk ceria. It is interesting that catalyst Pt/CeO_2/SBA-DP20 exhibits a markedly higher WGS activity than Pt/CeO_2/SBA-IMP20. The benefit of using CeO_2 nanoparticles embedded in SBA-15 pore channels as a support for Pt is obvious. We propose the following explanation for the enhanced activity of the Pt/CeO_2/SBA-DP20 catalyst. It is generally accepted that the WGS reaction over reducible oxide-supported NM catalysts occurs in a bifunctional manner with the participation of both the dispersed metal phase and the support. A so-called ceria-mediated redox mechanism [29] has been outlined, according to which CO adsorbed on the metal is oxidized to CO_2 by oxygen of the support, which in turn is reoxidized by water, releasing hydrogen. Assumed this redox mechanism is operable, the observed strong dependence of the WGS activity on the CeO_2 particle size may be related to the effect of size reduction on the CeO_2 redox properties. TPR results have verified that the reducibility of surface ceria depends strongly on the ceria domain size (particle size of CeO_2 crystallites).

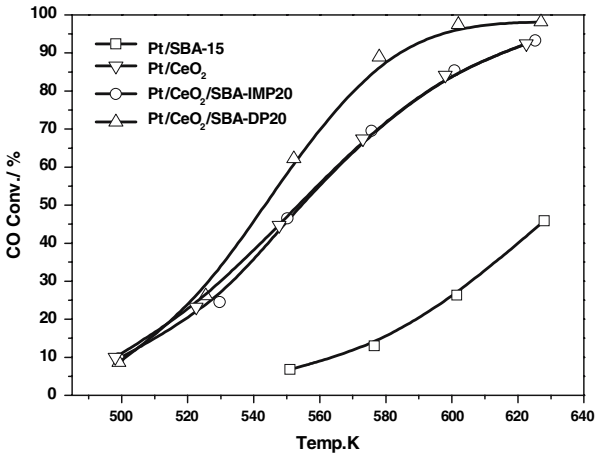

Fig. 7 Catalytic water-gas-shift (WGS) reaction activity evaluation of Pt catalyst supported on CeO2-modified SBA-15 as well as reference catalyst Pt/SBA-15 and Pt/CeO2 in terms of CO conversion versus temperature

If a synergetic mechanism occurs at the Pt and metal oxide interface, the characteristics of the metal oxide surface should be of paramount importance. In other words, if the support could be prepared in the form of discrete, well-defined nanoparticles, this should have an influence on the surface electronic properties and consequently on the Pt-support interaction [30]. Therefore, the fact that the CeO_2 support is in the form of nanocrystalline particles appears to be a key factor for achieving high activity in the WGS reaction.

3.5 Transmission Electron Microscopy Characterization

Figure 8 shows some TEM micrographs of the samples under investigation. In details, Fig. 8a presents a TEM

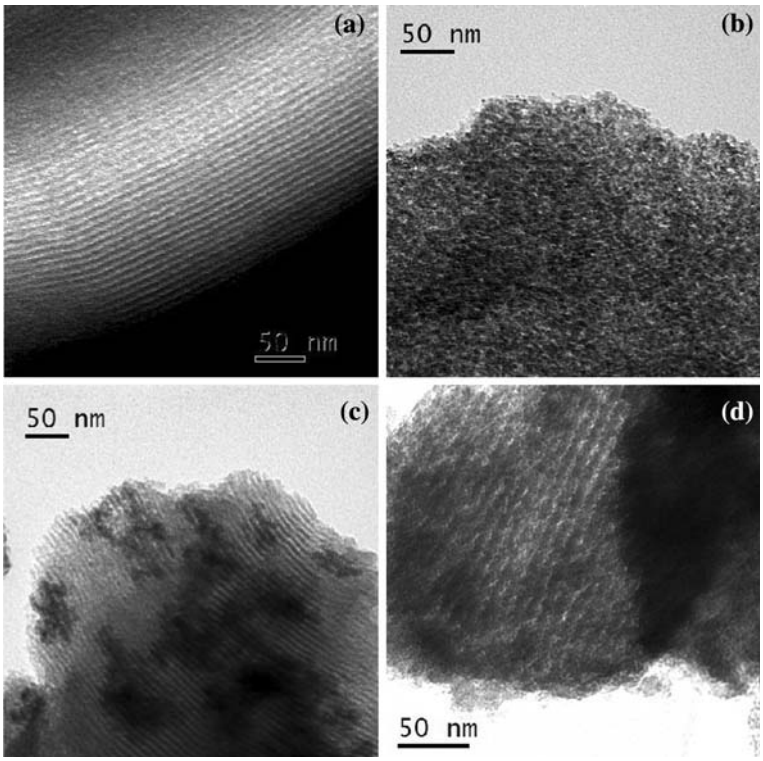

Fig. 8 Transmission electron micrograph of (**a**) SBA-15, (**b**) CeO2/SBA-DP20, (**c**) CeO2/SBA-IMP20, (**d**) Pt/CeO2/SBA-DP20 catalyst rafter 5 h WGS reaction

micrograph of the parent SBA-15 material, showing a uniform nanotubular mesoporous structure. The TEM micrograph of the CeO_2/SBA-DP20 sample is illustrated in Fig. 8b, showing homogeneous ceria distribution in SBA-15. It should be noted that when their main axis is perpendicular to the beam, alternating clear and dark stripes are not as obvious as that presented in parent SBA-15 sample. This phenomenon illuminates that the decreased electronic density contrasts between mesopores and silica walls, caused by the contraction of pore wall and the inclusion of ceria particles. In contrast, for the CeO_2/SBA-IMP20 sample shown in Fig. 8c, many large particles deposited on the external surface of SBA-15 were observed, suggesting that the ceria precursor were pulled out from the SBA-15 pores by capillary force during evaporation. Finally, Fig. 8d shows a TEM micrograph of Pt/CeO_2/SBA-DP20 catalyst after 5 h WGS reaction. No significant change can be observed compared to CeO_2/SBA-DP20 sample, which ensures the stability of the catalyst materials during catalytic operation.

4 Conclusion

Incipient wetness impregnation (IMP) and deposition precipitation (DP) methods were used to synthesize CeO_2 particles confined within the pores of SBA-15. Via DP nanocrystalline CeO_2 guest phases were located exclusively inside the SBA-15 pores, thereby resulting in a homogeneous CeO_2 particles distribution, which is opposite to that substantial pore blocking occurred during IMP. The catalytic activity of the Pt/CeO_2/SBA-15 catalyst for WGSR was greatly improved due to the CeO_2 particles nanosize and their effective interaction with Pt particles. This catalyst makes the process interesting from both an economic and environmental point of view.

References

1. Zalc JM, Sokolovskii V, Löffler DG (2002) J Catal 206:169
2. Liu XS, Ruettinger W, Xu XM, Farrauto R (2005) Appl Catal B Env 56:69
3. Goguet A, Meunier FC, Tibiletti D, Breen JP, Burch R (2004) J Phys Chem B 108:20240
4. Jacobs G, Grahama U, Chenua E, Pattersona P, Dozierb A, Davis B (2005) J Catal 229:499
5. Deng WL, Flytzani-Stephanopoulos M (2006) Angew Chem Int Ed 45:1
6. Fu Q, Saltsburg H, Flytzani-Stephanopoulos M (2003) Science 301:935
7. Yeung CMY, Yu KMK, Fu QJ, Thompsett D, Petch MI, Tsang SC (2005) J Am Chem Soc 127:18010
8. Zhang X, Wang H, Xu BQ (2005) J Phys Chem B 109:9678
9. Abad A, Concepci P, Corma A, Garc H (2005) Angew Chem Int Ed 44:4066
10. Panagiotopoulou P, Kondarides DI (2004) J Catal 225:327
11. Kresge CT, Leonowicz ME, Roth WJ, Vartuli JC, Beck JS (1992) Nature 359:710
12. Feng X, Fryxell GE, Wang LQ, Kim AY, Liu J, Kemner KM (1997) Science 276:923

13. Zhu HG, Liang CD, Yan WF, Overbury SH, Dai S (2006) J Phys Chem B 110:10842
14. Segura Y, Cool P, Van Der Voort P, Mees F, Meynen V, Vansant EF (2004) J Phys Chem B 108:3794
15. Xu W, Liao YT, Akins D (2002) J Phys Chem B 106:11127
16. Zhao D, Feng J, Huo Q, Melosh N, Fredrickson GH, Chmelka BF, Stucky GD (1998) Science 279:548
17. Schüth F, Wingen A, Sauer J (2001) Micropor Mesopor Mater 44–45:465
18. Gómez-Reynoso R, Ramírez J, Nares R, Luna R, Murrieta F (2005) Catal Today 107–108:926
19. Vråstad T, Magnusson HK, Sjölom J (2007) Micropor Mesopor Mater, doi: 10.1016/j.micromeso.2007.02.048
20. Perathoner S, Lanzafame P, Passalacqua R, Centi G, Schlogl R, Su DS (2006) Micropor Mesopor Mater 90:347
21. Vradman L, Landau MV, Kantorovich D, Koltypin Y, Gedanken A (2005) Micropor Mesopor Mater 79:307
22. Sonwane CG, Ludovice PJ (2005) J Mol Catal A Chem 238:135
23. Escax V et al (2007) Micropor Mesopor Mater 102:234
24. Yao HC, Yu Y (1984) J Catal 86:254
25. Giordano F, Trovarelli A, de Leitenburg C, Giona M (2000) J Catal 193:273
26. Concepcion P, Corma A, Silvestre-Albero J, Franco V, Chane-Ching JY (2004) J Am Chem Soc 126:5523
27. Yan WF, Chen B, Mahurin SM, Hagaman EW, Dai S, Overbury SH (2004) J Phys Chem B 108:2793
28. Trovarelli A (1996) Catal Rev Sci Eng 38:439
29. Gorte RJ, Zhao S (2005) Catal Today 104:18
30. Carrettin S, Concepcin P, Corma A, Lopez Nieto JM, Puntes VF (2004) Angew Chem Int Ed 43:2538